SINGLE vs MULTI-POLARIZATION INTERFEROMETRY

Kostas PAPATHANASSIOU[(1)], Shane R. CLOUDE[(2)]

[(1)]German Aerospace Center e.V. (DLR)
Microwaves and Radar Institute (DLR-HR)
SAR Technology Department, Pol-InSAR Research Group
P.O. Box 1116, D-82234 Wessling
Tel / Fax: +49 8153-28-2367 / 1135
e-mail: kostas.papathanassiou@dlr.de
web : www.dlr.de/HR

[(2)]AEL Consultants
26 Westfield Avenue, Cupar, Fife, KY15 5AA
Scotland, UK
Tel/Fax : +44 1334 650761
e-mail : scloude@ieee.org,
web : http://homepage.mac.com/aelc/

1 VECTOR FORMULATION OF INTERFEROMETRY

1.1 FORMING AN INTERFEROGRAM USING DIFFERENT POLARISATIONS

A monostatic, fully-polarimetric interferometric SAR system measures for each resolution element in the scene, from two slightly different look angles (see Figure 1), two scattering matrices, $[S_1]$ and $[S_2]$

$$[S_1]=\begin{bmatrix} S^1_{HH} & S^1_{HV} \\ S^1_{VH} & S^1_{VV} \end{bmatrix} \qquad \text{and} \qquad [S_2]=\begin{bmatrix} S^2_{HH} & S^2_{HV} \\ S^2_{VH} & S^2_{VV} \end{bmatrix} \tag{1}$$

Assuming reciprocal scattering, the corresponding three-dimensional Pauli-scattering vectors $\vec{k}_1$ and $\vec{k}_2$ are then given by

$$\vec{k}_1=\frac{1}{\sqrt{2}}[S^1_{HH}+S^1_{VV} \quad S^1_{HH}-S^1_{VV} \quad 2S^1_{HV}]^T$$
$$\text{and } \vec{k}_2=\frac{1}{\sqrt{2}}[S^2_{HH}+S^2_{VV} \quad S^2_{HH}-S^2_{VV} \quad 2S^2_{HV}]^T \tag{2}$$

The complete information measured by the SAR system can be represented in form of three 3x3 complex matrices $[T_{11}]$, $[T_{22}]$ and $[\Omega_{12}]$ formed using the outer products of the scattering vectors $\vec{k}_1$ and $\vec{k}_2$ as

$$[T_{11}] := < \vec{k}_1^{+} \cdot \vec{k}_1 > \qquad [T_{22}] := < \vec{k}_2^{+} \cdot \vec{k}_2 > \qquad [\Omega_{12}] := < \vec{k}_1^{+} \cdot \vec{k}_2 > \tag{3}$$

$[T_{11}]$ and $[T_{22}]$ are the conventional hermitian polarimetric coherency matrices, which describe the polarimetric properties for each individual image separately, while $[\Omega_{12}]$ is a non-

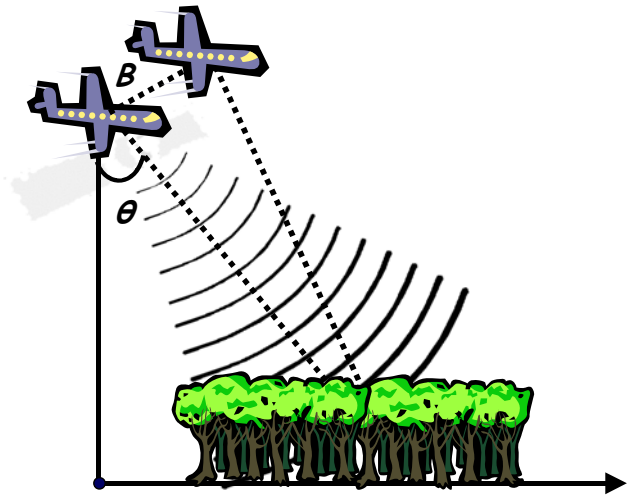

Figure 1 Pol-InSAR Acquisition Geometry.

hermitian complex matrix which contains polarimetric and interferometric information. The two complex (scalar) images i1 and i2 for forming the interferogram are obtained by projecting the scattering vectors $\vec{k}_1$ and $\vec{k}_2$ onto two unitary complex vectors $\vec{w}_1$ and $\vec{w}_2$, which define the polarisation of the two images respectively as

$$i_1 = \vec{w}_1^{+} \cdot \vec{k}_1 \qquad \text{and} \qquad i_2 = \vec{w}_2^{+} \cdot \vec{k}_2 \tag{4}$$

According to (4), i_1 and i_2 are linear combinations of the elements of the scattering matrices $[S_1]$ and $[S_2]$. The interferogram related to the polarisations given by $\vec{w}_1$ and $\vec{w}_2$ is then

$$i_1 \; i_2^{*} = (\vec{w}_1^{+} \cdot \vec{k}_1)(\vec{w}_2^{+} \cdot \vec{k}_2)^{+} = \vec{w}_1 (\vec{k}_1 \cdot \vec{k}_2^{+}) \vec{w}_2^{+} = \vec{w}_1 [\Omega] \vec{w}_2^{+} \tag{5}$$

and the corresponding interferometric phase follows as

$$\varphi = \arg(i_1 \; i_2^{*}) = \arg(\vec{w}_1 (\vec{k}_1 \cdot \vec{k}_2^{+}) \vec{w}_2^{+}) = \arg(\vec{w}_1 [\Omega] \vec{w}_2^{+}) \tag{6}$$

Finally, using (4) and (5), the complex interferometric coherence as a function of the polarisation of the two images may be written as

$$\tilde{\gamma}(\vec{w}_1, \vec{w}_2) = \frac{< i_1 \; i_2^{*} >}{\sqrt{< i_1 \; i_1^{*} > \; < i_2 \; i_2^{*} >}} = \frac{< \vec{w}_1 [\Omega] \vec{w}_2^{+} \; >}{\sqrt{< (\vec{w}_1 [T] \vec{w}_1^{+} \;) > \; < (\vec{w}_2 [T] \vec{w}_2^{+} \;) >}} \tag{7}$$

with $|\tilde{\gamma}(\vec{w}_1, \vec{w}_2)| \leq 1$. For convenience, we will distinguish in the following between the conventional coherence coefficient $\gamma(\vec{w}_1, \vec{w}_2) = |\tilde{\gamma}(\vec{w}_1, \vec{w}_2)|$ and the complex coherence $\tilde{\gamma}(\vec{w}_1, \vec{w}_2) = \gamma(\vec{w}_1, \vec{w}_2) \exp(i\varphi)$ that includes additional to the coherence coefficient the interferometric phase.

There are two cases to be distinguished:

- $\vec{w}_1 = \vec{w}_2$, i.e., images with the same polarisation are used to form the interferogram: In this case, the interferometric phase (6) contains only the interferometric contribution due to the topography and range variation while the interferometric coherence (7) expresses the interferometric correlation behaviour.
- $\vec{w}_1 \neq \vec{w}_2$, i.e., images with different polarisation are used to form the interferogram: In this case, the interferometric phase (6) contains beside the interferometric also the phase difference between the two polarisations. The interferometric coherence expresses apart from the interferometric correlation behaviour also the polarimetric correlation between the two polarisations

$$\tilde{\gamma}(\vec{w}_1, \vec{w}_2) = \tilde{\gamma}_{Int} \cdot \tilde{\gamma}_{Pol} \tag{8}$$

where

$$\tilde{\gamma}_{Pol}(\vec{w}_1, \vec{w}_2) = \frac{< \vec{w}_1 [T] \vec{w}_2^{+} \; >}{\sqrt{< (\vec{w}_1 [T] \vec{w}_1^{+} \;) > \; < (\vec{w}_2 [T] \vec{w}_2^{+} \;) >}} \tag{9}$$

Example 1: *HH-HH inteferogram generation*

1. Chose $\vec{w}_1 = \frac{1}{\sqrt{2}} [1 \quad -1 \quad 0]^T$ and $\vec{w}_2 = \frac{1}{\sqrt{2}} [1 \quad -1 \quad 0]^T$
2. Project the scattering vectors formed for Image 1 & 2 onto the chosen $\vec{w}_1$ & $\vec{w}_2$

   $S_{HH}^1 = \vec{w}_1^{+} \cdot \vec{k}_1$ and $S_{HH}^2 = \vec{w}_2^{+} \cdot \vec{k}_2$

3. Interferogram formation:

$$i_1 \quad i_2^* = (\vec{w}_1^{\,+} \cdot \vec{k}_1)(\vec{w}_2^{\,+} \cdot \vec{k}_2)^+ = \vec{w}_1[\Omega]\vec{w}_2^{\,+} = S_{HH}^{1} \quad S_{HH}^{2*}$$

4. Interferometric phase:

$$\varphi = \arg(\, i_1 \quad i_2^*) = \arg(\, \vec{w}_1[\Omega]\vec{w}_2^{\,+}) = \arg(\, S_{HH}^{1} \quad S_{HH}^{2*}\,)$$

5. Interferometric coherence:

$$\tilde{\gamma}(\vec{w}_1, \vec{w}_2) = \frac{< \vec{w}_1[\Omega]\vec{w}_2^{\,+} \;>}{\sqrt{< (\vec{w}_1[T]\vec{w}_1^{\,+}) > < (\vec{w}_2[T]\vec{w}_2^{\,+}) >}} = \frac{< S_{HH}^{1} \quad S_{HH}^{2*} >}{\sqrt{< S_{HH}^{1} \quad S_{HH}^{1*} > < S_{HH}^{2} \quad S_{HH}^{2*} >}}$$

Example 2:

The Oberpfaffenhoffen (OP) test site is a mixed forest/urban/agricultural region surrounding the DLR center in Oberpfaffenhofen, near Munich in Germany. Figure 2 shows the L-band SAR amplitude images at three different polarisations, HH, HV=VH, and VV. The airfield Oberpfaffenhofen is located in the upper part of the image where the runway appears dark at all polarisations due to the almost specular scattering and the surrounding fields show a typical surface scattering behaviour with $|HV| \lessapprox |HH| \lessapprox |VV|$. The buildings of DLR and Dornier are located in the center of the image, while on the right hand side the village of Gilching appears. The forested area including homogeneous beech and pine stands of different ages and heights as well as mixed forest stands, starts directly on the lower edge of the industrial (DLR and Dornier) zone. Finally the lower part of the image is a mixed forest-agriculture land scene.

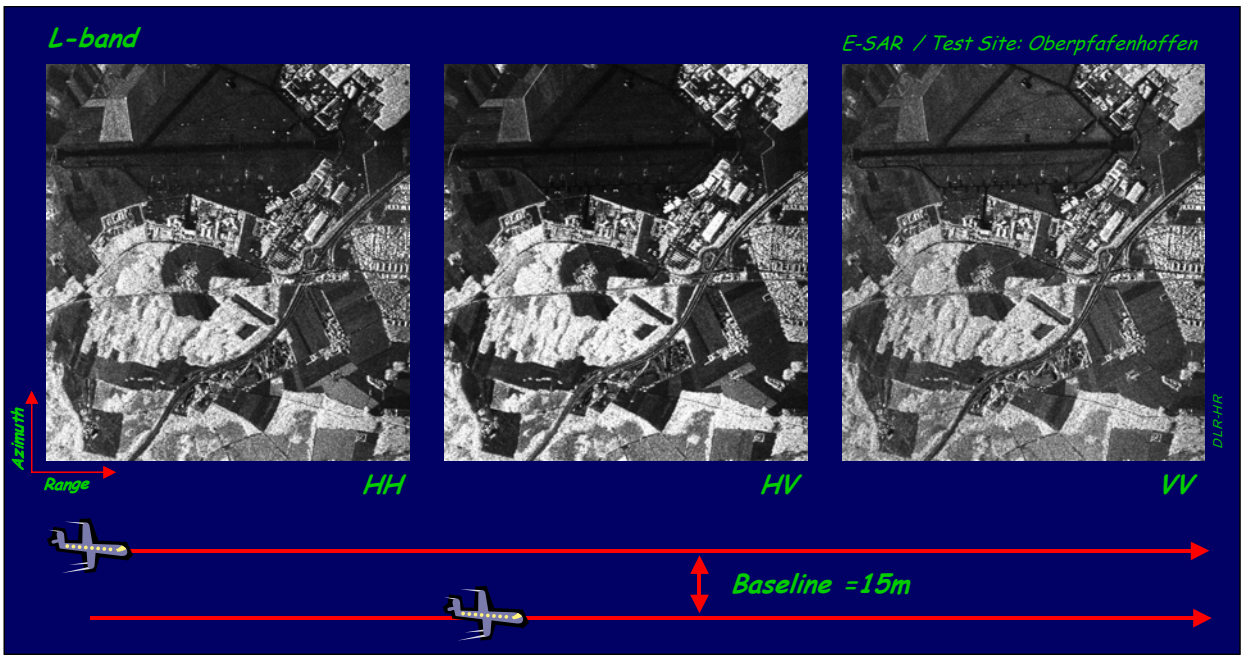

Figure 2 Left: HH, Middle: HV, Right: VV SAR images for the OP test site.

The conventional interferometric phase images are shown in Figure 3. A gentle slope from near- to far-range can be recognised. The top of the buildings and the forest appears with a different phase than their surroundings. However, there is no significant difference in the three phase patterns as the difference in the effective phase centers - if any - is not so big to become directly visible. The

different levels of phase noise at the different polarisations forebode different coherence images. Indeed, the corresponding coherence maps - obtained by using the conventional (HH, HV=VH, and VV) polarisation channels for forming the interferogram - are shown in Figure 4. Over the runway and the neighbouring fields the change of coherence with polarisation is primarily due to SNR effects, while the differences over the forested and vegetated areas are due to different volume decorrelation contributions. How they can be interpreted it will be discussed in the next sections.

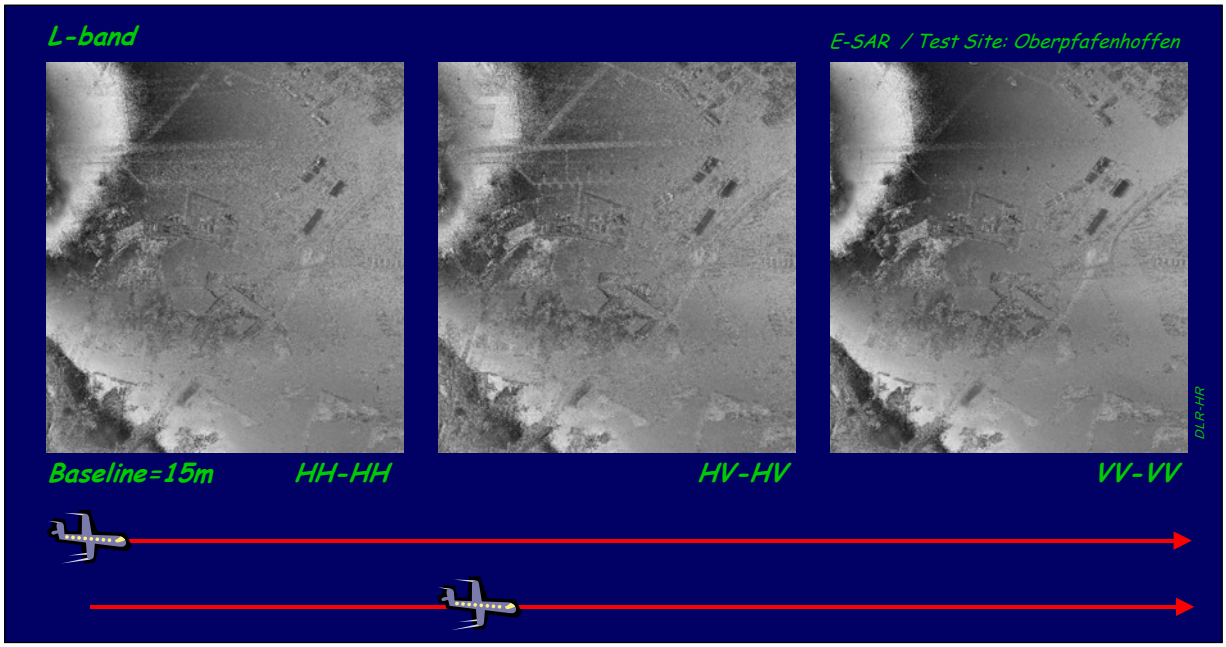

Figure 3 Left: HH-HH, Middle: HV-HV, Right: VV-VV interferometric phase images.

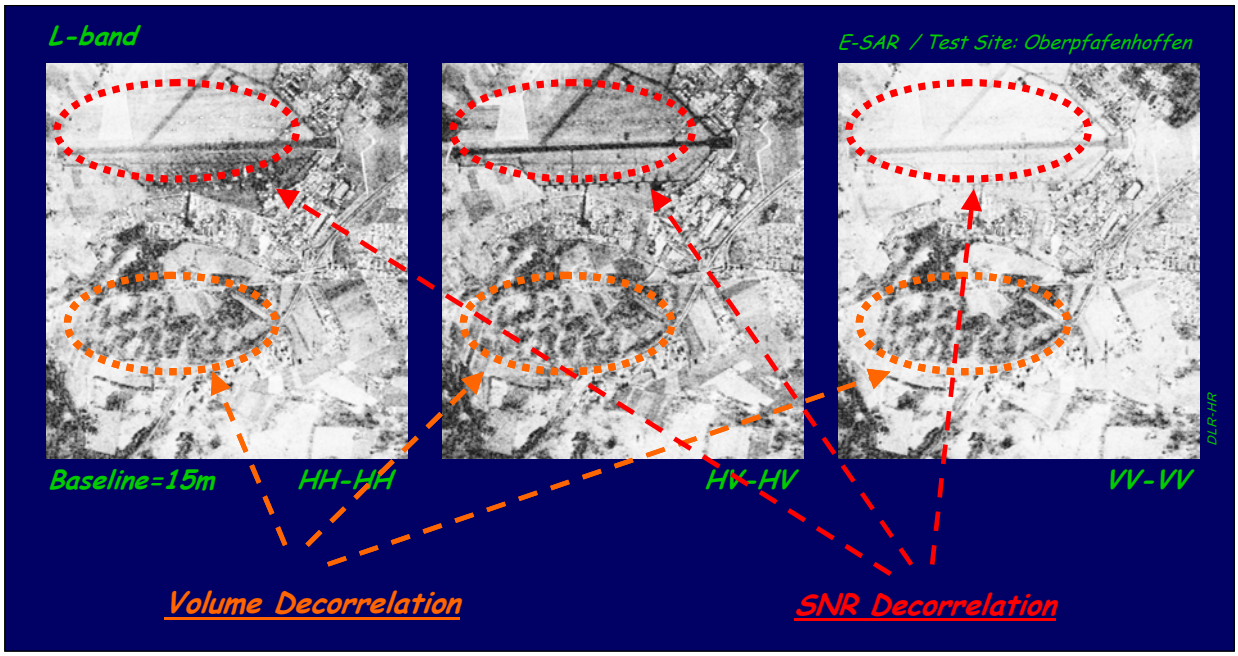

Figure 4 Left: HH-HH, Middle: HV-HV, Right: VV-VV interferometric coherence images.

1.2 CHANGE OF BASIS IN POLARIMETRIC INTERFEROMETRY

The knowledge of the scattering matrix in one polarisation basis allows us to derive the scattering matrix in any other orthogonal $\{\vec{\varepsilon}_A, \vec{\varepsilon}_B\}$ basis by unitary congruence transformations of the original matrix $[S]_{HV}$

$$[S]_{AB} = [U_2][S]_{HV}[U_2] \tag{10}$$

where the 3-parameter transformation matrix $[U_2]$ has the form

$$[U_2] = \frac{1}{\sqrt{1+\rho\rho^*}} \begin{bmatrix} 1 & -\rho^* \\ \rho & 1 \end{bmatrix} \begin{bmatrix} \exp(i\delta) & 0 \\ 0 & \exp(-i\delta) \end{bmatrix} \tag{11}$$

and where

$$\rho = \frac{\cos(2\chi)\sin(2\psi) + i\sin(2\chi)}{1 \_ \cos(2\chi)\cos(2\psi)} \tag{12}$$

is the complex polarisation ratio. The angles χ, ψ are the polarimetric ellipticity and orientation angles describing the new basis (i.e. for $\vec{\varepsilon}_A$) respectively. Equation (11) shows that if we wish to change the phase of the basis polarisation state A by an angle δ, then we must change the phase of the orthogonal B component by the negative of this angle. In radar polarimetry, the absolute knowledge of the phase reference δ was not important because it is not characteristic of the polarisation state of the wave. However, for interferometric applications the exact definition of phase is essential. The angle δ represents an absolute zero phase in the new polarimetric basis, and thus, the use of different δ angles for the transformation of the two scattering matrices $[S_1]$and $[S_2]$ will introduce a phase offset in the phase of the interferograms formed between their elements. To avoid this, it is important to use one and the same phase for the transformation of both images. In the following we will assume that $\delta = 0$ for the transformation of both images.

The corresponding transformation of the scattering vector $\vec{k}_{HV}$ is also given by a 3 x 3 special unitary matrix $[U_3]$

$$\vec{k}_{AB} = [U_3]\vec{k}_{HV} \tag{13}$$

with

$$[U_3] = \frac{1}{2(1+\rho\rho^*)} \begin{bmatrix} 2+\rho^2+\rho^{*2} & \rho^{*2}-\rho^2 & 2(\rho-\rho^*) \\ \rho^2-\rho^{*2} & 2-(\rho^2+\rho^{*2}) & 2(\rho+\rho^*) \\ 2(\rho-\rho^*) & -2(\rho+\rho^*) & 2(1-\rho\rho^*) \end{bmatrix} \tag{14}$$

The possibility of transforming the scattering vector into any orthogonal polarimetric basis allows us to form interferograms between all possible elliptical polarisation states. After transforming both scattering vectors, $\vec{k}_1$ and $\vec{k}_2$, from the $\{\vec{\varepsilon}_H, \vec{\varepsilon}_V\}$ basis into the $\{\vec{\varepsilon}_A, \vec{\varepsilon}_B\}$ basis we obtain the complex scattering coefficients corresponding to the polarisations in the new basis by forming their projections onto normalised complex vectors $\vec{w}_i$,

$$i_1 = \vec{w}_1^+ \cdot \vec{k}_{1AB} = \vec{w}_1^+ \cdot [U_3]\vec{k}_{1AB} \qquad \text{and} \qquad i_2 = \vec{w}_2^+ \cdot \vec{k}_{2AB} = \vec{w}_2^+ \cdot [U_3]\vec{k}_{2AB} \tag{15}$$

The interferogram formation is then described by

$$\begin{aligned} i_1\ \ i_2^* &= (\vec{w}_1^{+}\cdot\vec{k}_{1AB})(\vec{w}_2^{+}\cdot\vec{k}_{2AB})^{+} \\ &= (\vec{w}_1^{+}\cdot[U_3]\vec{k}_{1hv})(\vec{w}_2^{+}\cdot[U_3]\vec{k}_{1hv})^{+} = \vec{w}_1^{+}[U_3][\Omega][U_3]^{+}\vec{w}_2 \end{aligned} \tag{16}$$

Comparing the last equation with (5), we recognise that interferogram formation in any polarisation basis may be described by an unitary similarity transformation of the $[\Omega]$ matrix! The interferometric phase in the new basis is then given by

$$\varphi = \arg(i_1\ \ i_2^*) = \arg(\vec{w}_1^{+}[U_3][\Omega][U_3]^{+}\vec{w}_2) \tag{17}$$

and the corresponding interferometric coherence results as

$$\begin{aligned} \tilde{\gamma}(\vec{w}_1,\vec{w}_2) &= \frac{<i_1\ i_2^*>}{\sqrt{<i_1\ i_1^*><i_2\ i_2^*>}} \\ &= \frac{<\vec{w}_1^{+}[U_3][\Omega][U_3]^{+}\vec{w}_2>}{\sqrt{<(\vec{w}_1^{+}[U_3][T_{11}][U_3]^{+}\vec{w}_1)><\vec{w}_2^{+}[U_3][T_{22}][U_3]^{+}\vec{w}_2>}} \end{aligned} \tag{18}$$

Physically, $[U_3]$ polarimetric transformations correspond to changes in the selected scattering mechanism within the image. Changing the polarisation of an image changes the effective scatterers and/or their relative contributions and leads to different scattering distributions. They again affect in a direct way the interferometric coherence as it will be discussed in the next sections.

Example 1: *Transformation from the measured H/V linear polarised basis* $\{\vec{\varepsilon}_H,\vec{\varepsilon}_V\}$*, into the Left-/Right-hand circular polarisation basis* $\{\vec{\varepsilon}_L,\vec{\varepsilon}_R\}$, and *LL-LL inteferogram generation.*

1. Left circular polarisation is defined in terms of the polarisation angles by $\psi = 0^o$ and $\chi = 45^o$. From (12) follows the corresponding complex polarisation ratio as $\rho = i$.
2. Using (14) we obtain the unitary matrix $[U_3]$ as

$$[U_3] = \begin{bmatrix} 0 & 0 & i \\ 0 & 1 & 0 \\ i & 0 & 0 \end{bmatrix}$$

3. The scattering vectors $\vec{k}_{LR(i=1,2)}$ in the $\{\vec{\varepsilon}_L,\vec{\varepsilon}_R\}$ basis are then given as

$$\vec{k}_{LR} = [U_3]\vec{k}_{HV} \rightarrow \begin{bmatrix} S_{LL}^{i=1,2}+S_{RR}^{i=1,2} \\ S_{LL}^{i=1,2}-S_{RR}^{i=1,2} \\ 2S_{LR}^{i=1,2} \end{bmatrix} = \begin{bmatrix} 0 & 0 & i \\ 0 & 1 & 0 \\ i & 0 & 0 \end{bmatrix}\begin{bmatrix} S_{HH}^{i=1,2}+S_{VV}^{i=1,2} \\ S_{HH}^{i=1,2}-S_{VV}^{i=1,2} \\ 2S_{HV}^{i=1,2} \end{bmatrix} = \begin{bmatrix} 2iS_{HV}^{i=1,2} \\ S_{HH}^{i=1,2}-S_{VV}^{i=1,2} \\ i*(S_{HH}^{i=1,2}+S_{VV}^{i=1,2}) \end{bmatrix}$$

4. Chose $\vec{w}_1 = \frac{1}{\sqrt{2}}[1\ \ -1\ \ 0]^T$ and $\vec{w}_2 = \frac{1}{\sqrt{2}}[1\ \ -1\ \ 0]^T$
5. Project the scattering vectors in the $\{\vec{\varepsilon}_L,\vec{\varepsilon}_R\}$ basis onto the chosen $\vec{w}_1$ & $\vec{w}_2$:

$$S_{LL}^{1} = \vec{w}_1^{+} \cdot \vec{k}_1 \qquad \text{and} \qquad S_{LL}^{2} = \vec{w}_2^{+} \cdot \vec{k}_2$$

6. Interferogram formation:

$$i_1 \;\; i_2^{*} = (\vec{w}_1^{+} \cdot \vec{k}_1)(\vec{w}_2^{+} \cdot \vec{k}_2)^{+} = \vec{w}_1[\Omega]\vec{w}_2^{+} = S_{LL}^{1} \;\; S_{LL}^{2*}$$

7. Interferometric phase:

$$\varphi = \arg(i_1 \;\; i_2^{*}) = \arg(\vec{w}_1[\Omega]\vec{w}_2^{+}) = \arg(S_{LL}^{1} \;\; S_{LL}^{2*})$$

8. Interferometric coherence:

$$\tilde{\gamma}(\vec{w}_1, \vec{w}_2) = \frac{< \vec{w}_1[\Omega]\vec{w}_2^{+} \; >}{\sqrt{< (\vec{w}_1[T]\vec{w}_1^{+} \;) > \; < (\vec{w}_2[T]\vec{w}_2^{+} \;) >}} = \frac{< S_{LL}^{1} \;\; S_{LL}^{2*} >}{\sqrt{< S_{LL}^{1} \;\; S_{LL}^{1*} > \; < S_{LL}^{2} \;\; S_{LL}^{2*} >}}$$

1.3 COHERENCE OPTIMISATION

The dependency of the interferometric coherence on the polarisation of the images used to form the interferogram – expressed by $\vec{w}_1$ and $\vec{w}_2$ - leads us to consider the question of which polarisation yields the highest coherence. While much work has been carried out on optimisation theory in polarimetry, all of it has been addressed to the single image or non-coherent cases. In order to solve the interferometric optimisation problem, a coherent (i.e., phase preserving) optimisation method is required.
The problem is to optimise the general formulation of the interferometric coherence as given in (7). Mathematically, this can be done by maximising the complex Lagrangian function L defined as

$$L := \vec{w}_1[\Omega_{12}]\vec{w}_2^{+} + \lambda_1(\vec{w}_1[T_{11}]\vec{w}_1^{+} - C_1) + \lambda_2(\vec{w}_2[T_{22}]\vec{w}_2^{+} - C_2) \tag{19}$$

C_1 and C_2 are constants, and λ_1 and λ_2 are Lagrange multipliers introduced in order to maximise the numerator of (7) while keeping the denominator constant. Since L is complex, the maximisation problem is of the form

$$\max_{\vec{w}_1, \vec{w}_2} \{ \; L \;\; L^{*} \; \} \tag{20}$$

However, because $[T_{11}]$ and $[T_{22}]$ are by definition hermitian, the two terms on the right hand side of (19) are always real and the optimisation of L L^{*} may be reduced to optimisation of L. This simplifies the procedure, as no higher order products are required. We solve this maximisation problem by equating the partial derivatives to zero

$$\begin{aligned} \frac{\partial L}{\partial \vec{w}_1^{+}} &= [\Omega_{12}] \;\; \vec{w}_2 + \lambda_1[T_{11}]\vec{w}_1 = 0 \;\; \rightarrow \;\; \vec{w}_1^{+}[\Omega_{12}] \;\; \vec{w}_2 = -\lambda_1 \vec{w}_1^{+}[T_{11}]\vec{w}_1 \\ \frac{\partial L}{\partial \vec{w}_2^{+}} &= [\Omega_{12}]^{+}\vec{w}_1 + \lambda_2^{*}[T_{22}]\vec{w}_2 = 0 \;\; \rightarrow \;\; \vec{w}_2^{+}[\Omega_{12}]^{+}\vec{w}_1 = -\lambda_2^{*}\vec{w}_2^{+}[T_{22}]\vec{w}_2 \end{aligned} \tag{21}$$

By eliminating $\vec{w}_1$ or $\vec{w}_2$ respectively, (21) leads to two coupled 3x3 complex eigenvalue problems with common eigenvalues $\nu = \lambda_1\lambda_2^{*}$

$$\begin{aligned} [T_{22}]^{-1}[\Omega_{12}]^{+}[T_{11}]^{-1}[\Omega_{12}] \;\; \vec{w}_2 &= [A][B]\vec{w}_2 = \lambda_1\lambda_2^{*}\vec{w}_2 = \nu \;\; \vec{w}_2 \\ [T_{11}]^{-1}[\Omega_{12}] \;\; [T_{22}]^{-1}[\Omega_{12}]^{+}\vec{w}_1 &= [B][A]\vec{w}_1 = \lambda_1\lambda_2^{*}\vec{w}_1 = \nu \;\; \vec{w}_1 \end{aligned} \tag{22}$$

where $[A]=[T_{22}]^{-1}[\Omega_{12}]^{+}$ and $[B]=[T_{11}]^{-1}[\Omega_{12}]$. The two matrices [A][B] and [B][A] are similar, because $[A][B]=[A]([B][A])[A]^{-1}$, and therefore, have the same eigenvalues. Further, although both are not hermitian matrices, they are similar to hermitian positive semi-definite matrices, and hence, their eigenvalues are real non-negative.
Consequently, the two 3 x 3 complex eigenvector equations of (22) yield three real non-negative eigenvalues v_i (i=1,2,3) with $1 \geq v_1 \geq v_2 \geq v_3 \geq 0$. The optimum interferometric coherence values are then given by the square root of the corresponding eigenvalues

$$1 \geq \gamma_{opt1} = \sqrt{v_{opt1}} \geq \gamma_{opt2} = \sqrt{v_{opt2}} \geq \gamma_{opt3} = \sqrt{v_{opt3}} \geq 0 \tag{23}$$

The maximum possible coherence value γ_{opt1} that can be obtained by varying the polarisation is given by the square root of the maximum eigenvalue. Each eigenvalue is related to a pair of eigenvectors $\{\vec{w}_{1i}, \vec{w}_{2i,}\}$, one for each image. The first vector pair, $\{\vec{w}_{11}, \vec{w}_{21,}\}$, related to the largest singular value, represents the optimum polarisations, derived in the complete three-dimensional complex space of the vectors $\vec{\kappa}_i$. The second and third pairs $\{\vec{w}_{12}, \vec{w}_{22}\}$ and $\{\vec{w}_{13}, \vec{w}_{23}\}$, belonging to the second and third highest singular values, represent optimum solutions in different polarimetric subspaces.
The three optimum interferograms are obtained by projecting the scattering vectors $\vec{k}_1$ and $\vec{k}_2$ onto $\vec{w}_{opt1i}$ or $\vec{w}_{opt2i}$ in order to derive the optimum complex images i_{opt1i} and i_{opt2i}

$$i_{opt1i} = \vec{w}^{+}_{opt1i} \cdot \vec{k}_1 \quad \text{and} \quad i_{opt2i} = \vec{w}^{+}_{opt2i} \cdot \vec{k}_2 \tag{24}$$

However, before forming the interferogram, one note of caution is required. The absolute phase of the eigenvectors is not uniquely defined by (22) and so, an additional condition that fixes the phase difference between $\vec{w}_{opt1i}$ and $\vec{w}_{opt2i}$ uniquely has to be introduced. Looking at (6) we see that the interferometric phase information should be extracted from $\vec{k}_1 \cdot \vec{k}_2^{+}$. Hence a sensible constraint is to require

$$\arg(\ \vec{w}_{opt1i} \cdot \vec{w}_{opt2i}\ ) = 0 \tag{25}$$

This condition is automatically satisfied for $\vec{w}_{opt1i} = \vec{w}_{opt2i}$. When $\vec{w}_{opt1i} \neq \vec{w}_{opt2i}$ the phase difference between $\vec{w}_{opt11}$ and $\vec{w}_{opt12}$ can be estimated by

$$\varphi_e = \arg(\ \vec{w}_{opt1i} \cdot \vec{w}_{opt2i}\ ) \tag{26}$$

and removed from the individual images before forming the interferogram.

$$i_{opt1i} = i_{opt1i} \exp(-i\varphi_e / 2) \quad \text{and} \quad i_{opt2i} = i_{opt2i} \exp(+i\varphi_e / 2) \tag{27}$$

The corresponding optimum interferogram is then obtained as

$$i_{opt1i} i^{*}_{opt2i} = (\vec{w}_{opt1i} \cdot \vec{k}_1)(\vec{w}_{opt2i} \cdot \vec{k}_2)^{+} = \vec{w}_{opt1i}[\Omega]\vec{w}^{+}_{opt2i} \tag{28}$$

The three optimum complex coherences can be obtained from

$$\tilde{\gamma}_{opti}(\vec{w}_{opt1i},\vec{w}_{opt2i})=\frac{<i_{opt1i}\ i^{*}_{opt2i}>}{\sqrt{<i_{opt1i}i^{*}_{opt1i}><i_{opt2i}i^{*}_{opt2i}>}}=\frac{<\vec{w}_{opt1i}[\Omega]\vec{w}^{+}_{opt2i}>}{\sqrt{<(\vec{w}_{opt1i}[T]\vec{w}^{+}_{opt1i})><(\vec{w}_{opt2i}[T]\vec{w}^{+}_{opt2i})>}} \quad (29)$$

or directly by using the estimated eigenvalues

$$\tilde{\gamma}_{opti}(\vec{w}_{opt1i},\vec{w}_{opt2i})=\sqrt{v_{opti}}\exp(i\arg(i_{opt1i}i^{*}_{opt2i}))=\sqrt{v_{opti}}\exp(i\arg(\vec{w}_{opt1i}[\Omega]\vec{w}^{+}_{opt2i})) \quad (30)$$

The existence of solutions in (22) depends on the existence of the inverse matrices $[T_{11}]^{-1}$ and $[T_{22}]^{-1}$. This is not a severe constraint, as coherency matrices of distributed scatterers are in general of full rank 3. If, however, there happens to be a strongly polarised signal and the covariance matrices are of rank 2 or less, then the above formulation reduces to a two- or one-dimensional problem.

It is important to realise that the resulting optima are not the same optimum states as are well known in conventional polarimetric optimisation analysis. Polarimetric Signal-to-Noise optimisation of both images plays only a secondary role in the solution of the coherence optimisation problem because it accounts only for the contribution of SNR decorrelation. On the contrary, the coherence optimisation algorithm of Equation 20 deals mainly with volume decorrelation effects.

Example:

The three optimum interferometric coherence images obtained from the Oberpfaffenhofen area are shown in Figure 5. Comparing Figure x with Figure x makes clear that the maximised coherence values (Opt 1) are significantly higher than the coherence values obtained at any of the conventional polarisations over the whole image, including forested/vegetated as well as bare terrain types. While the coherence improvement over surface scatterers (runway, grass-land around the runway, bare fields in the upper and lower image part) is mainly due to SNR optimisation the coherence improvement over the forested areas (as it will be discussed latter on) arises by optimising the volume decorrelation component.

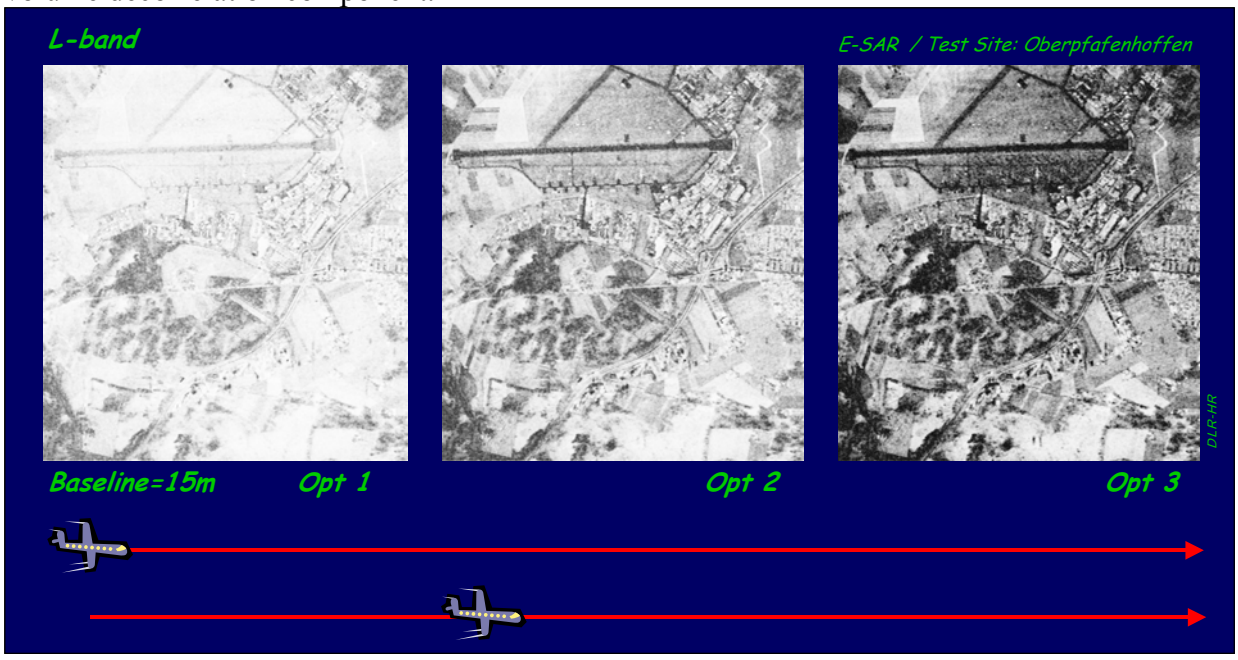

Figure 5 Left: Opt 1, Middle: Opt 2, Right: Opt 3 interferometric coherence images.

2 RELATING COHERENCE TO PHYSICAL STRUCTURE PARAMETERS

In this section the effect of vertical structure on the main Pol-InSAR observables - i.e. the interferometric phase and coherence at different polarisations - is discussed in terms of canonical scattering scenarios.

2.1 SURFACE SCATTERING AND INTERFEROMETRIC COHERENCE

Surface scatterers (see Figure 6 left) are impenetrable scatterers characterised by an isolated phase center in the vertical direction (i.e. z direction) so that - after range spectral filtering (i.e., $\gamma_{Range} = 1$) - geometrical decorrelation is no longer an issue (i.e. $\gamma_{Vol} = 1$). In other words, the interferometric coherence becomes independent of the baseline. In this case, the overall interferometric coherence becomes

$$\tilde{\gamma}(\vec{w}) = \gamma_{SNR}(\vec{w})\ \gamma_{Temp}(\vec{w}) \tag{31}$$

Accordingly, decorrelation over surfaces is due to SNR and temporal decorrelation. Both can be a function of polarisation. For single-pass systems, the only remaining decorrelation term is the SNR decorrelation

$$\gamma_{SNR}(\vec{w}) = \frac{1}{1 + \frac{N}{S(\vec{w})}} \tag{32}$$

where N is the Noise Equivalent Sigma Zero system level and S the backscattering power at a given polarisation $\vec{w}$. $S(\vec{w})$ depends - in first order - on the ratio of the system wavelength to the roughness dimensions of the surface and on its dielectric constant.

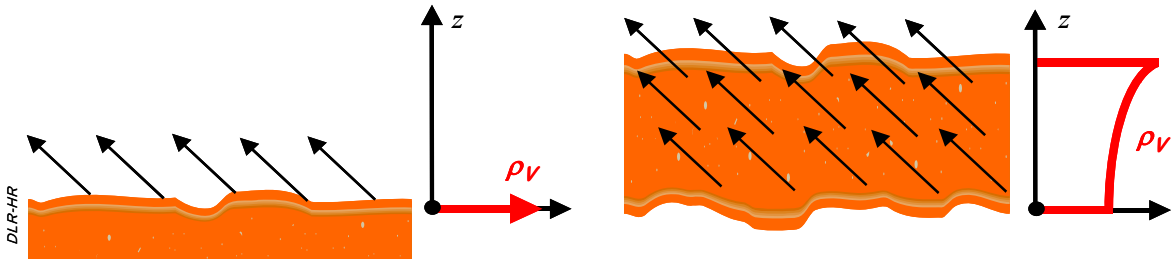

Figure 6 Surface vs Volume Scattering.

2.2 VOLUME SCATTERING AND INTERFEROMETRIC COHERENCE

Vegetation (forest as well as agriculture), land and see ice, as well as sand are some typical natural volume scatterers. Different as surface scatterers, volume scatterers are getting penetrated by the incidence wave and interact with it as a whole (see Figure 6 right). Accordingly, they are characterised by a finite vertical distribution of scatterers and as a direct consequence, they are affected by geometrical decorrelation in form of volume decorrelation ($|\tilde{\gamma}_{Vol}| < 1$). The interferometric coherence - after range spectral filtering (i.e., $\gamma_{Range} = 1$) - can be written as

$$\tilde{\gamma}(\vec{w}) = \gamma_{SNR}(\vec{w})\ \gamma_{Temp}(\vec{w})\ \tilde{\gamma}_{Vol}(\vec{w}) \tag{33}$$

The key term here is the volume decorrelation term $\tilde{\gamma}_{Vol}$ that depends directly on the vertical structure of the volume scatterer: Indeed, $\tilde{\gamma}_{Vol}$ - after range spectral filtering - is given by the (normalised) Fourier transformation of the vertical distribution of the effective scatterers $\rho_V(z)$ as

$$\tilde{\gamma}_{Vol} = \frac{\int \rho_V(z')\exp(-2i\kappa_z z')dz'}{\int \rho_V(z')dz'} \tag{34}$$

where κ_z is the effective vertical interferometric wavenumber after range spectral filtering, which depends on the imaging geometry and the radar wavelength

$$\kappa_z = \frac{\kappa\Delta\theta}{\sin(\theta)} \tag{35}$$

where $\kappa = 4\pi/\lambda$, θ the reference incidence angle and $\Delta\theta$ the incidence angle difference between the two interferometric images induced by the baseline.
Regarding the simplest case of a uniform vertical distribution of scatterers with height h_V

$$\rho_V(z) = rect\left(\frac{z}{h_V}\right) \tag{36}$$

the volume decorrelation contribution becomes

$$\tilde{\gamma}_{Vol} = \exp(k_z h_V/2)\frac{\sin(k_z h_V/2)}{k_z h_V/2} \tag{37}$$

This is the well-known $\sin(x)/x$ decorrelation behaviour. In this case, the phase center is located on the half height of the volume.
A more realistic volume scattering description has to include attenuation of the wave propagating through the volume medium (due to scattering and absorption). In this case the vertical distribution of scatterers $\rho_V(z)$ is given by

$$\rho_V(z) = \exp(z\sigma/\cos(\theta)) \tag{38}$$

where σ is the wave extinction coefficient corresponding to a mean extinction value for the volume layer expressing both scattering and absorption losses. It is primarily a function of the density of scatterers in the volume and their dielectric constant. For a volume height of h_V the volume decorrelation becomes

$$\tilde{\gamma}_{Vol} = \frac{\int_0^{h_V} \exp(z\sigma/\cos(\theta))\exp(-2i\kappa_z z')dz'}{\int_0^{h_V} \exp(z\sigma/\cos(\theta))dz'} \tag{39}$$

Based on the polarimetric dependency of the wave extinction coefficient σ the following two cases can be distinguished

- ***Random Volume (RV):*** The wave extinction is independent of polarisation: $\sigma \neq \sigma(\vec{w})$
- ***Oriented Volume (OV):*** The wave extinction changes with polarisation: $\sigma = \sigma(\vec{w})$.

These two cases will be discussed in the next sections.
Note that the coherence of a volume scatterer depends on the interferometric baseline (i.e. the vertical wave-number κ_z) due to the presence of the volume decorrelation contribution. SNR decorrelation is due to the higher backscatter of volume scatterers in general of secondary importance - at least for conventional InSAR systems.

Example:
Volume vs Surface Scattering
A two baseline repeat-pass InSAR data set at L-band (VV polarisation) acquired over the Oberpfaffenhofen test site is used to demonstrate the differences between surface and volume scatterers on the interferometric coherence. Figure 7 shows the three SAR amplitude images acquired along the three different tracks, as indicated. The interferometric phase images for the three resulting baselines are shown in Figure 8 where the increase of height sensitivity of the interferometric phase with increasing baseline becomes obvious. The corresponding coherence maps - after range spectral filtering - are shown in Figure 9. The degradation of the interferometric coherence with increasing baseline - as predicted for volume scatterers - can be seen over the forested and general vegetated areas. On the other hand, for the surface scattering areas (as the runway and its surrounding area) the coherence - as expected - does not change with baseline. While the surrounding fields have a coherence that equals 1 (as expected due to $\gamma_{Range} = 1$) the runway itself has a lower but still baseline independent coherence due to SNR decorrelation.

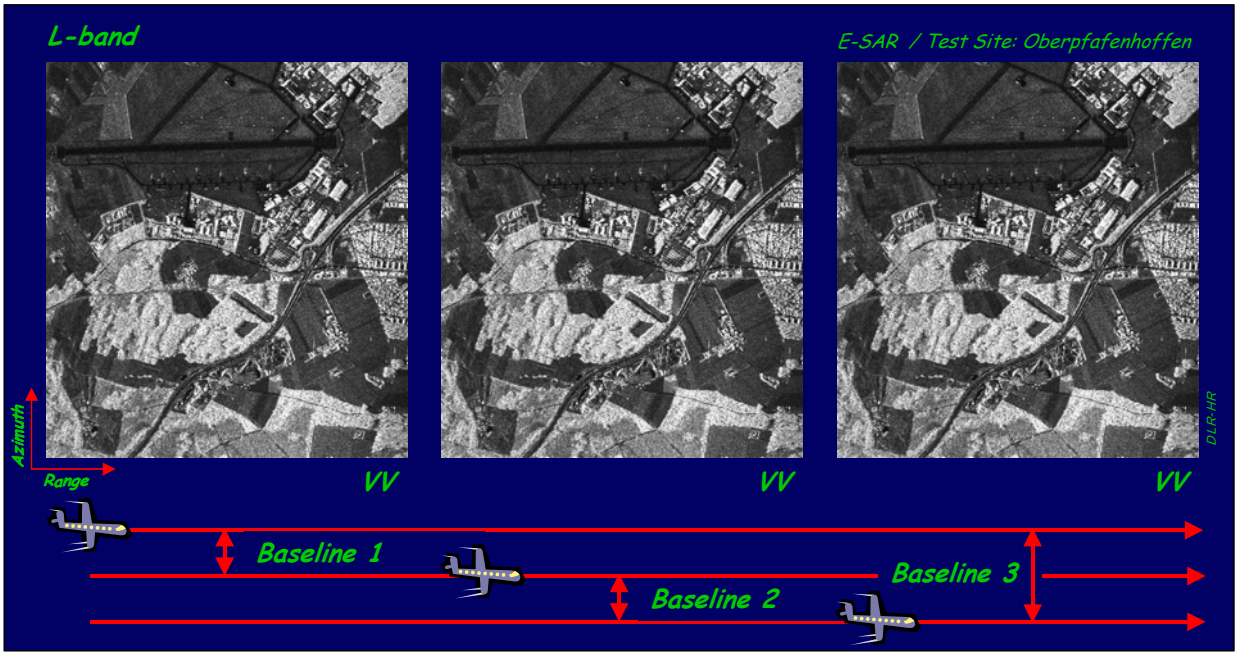

Figure 7 L-band VV polarised SAR images of the OP test site acquired along three slightly displaced tracks.

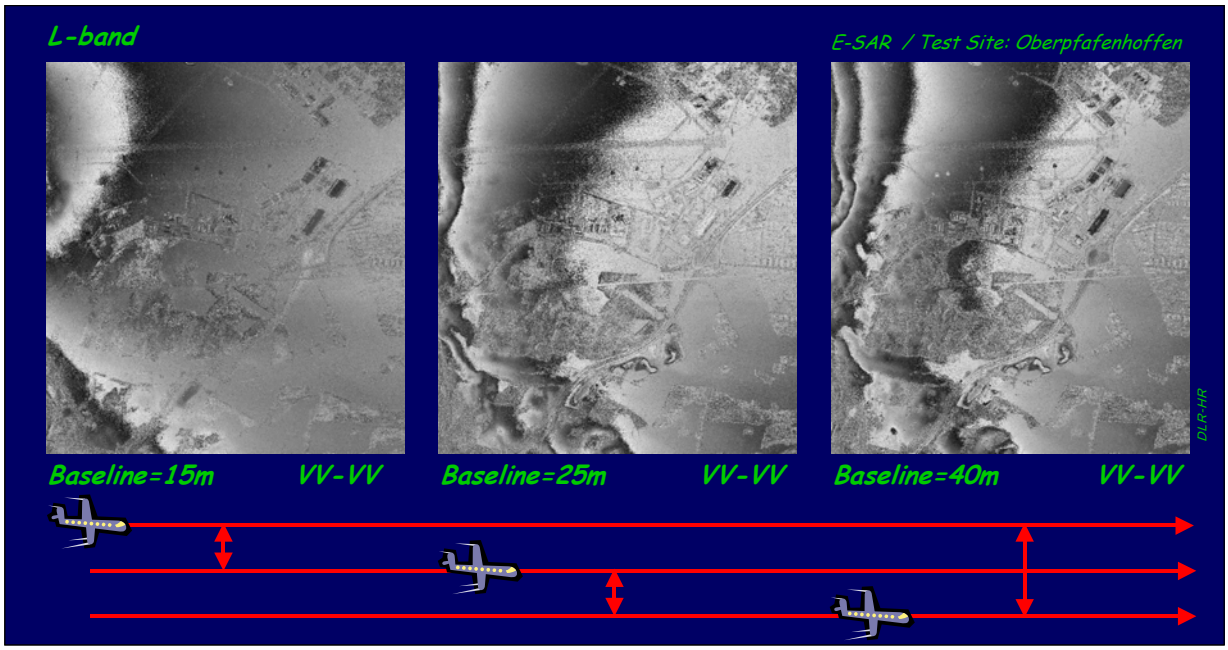

Figure 8 Interferometric phase images at three different baselines.

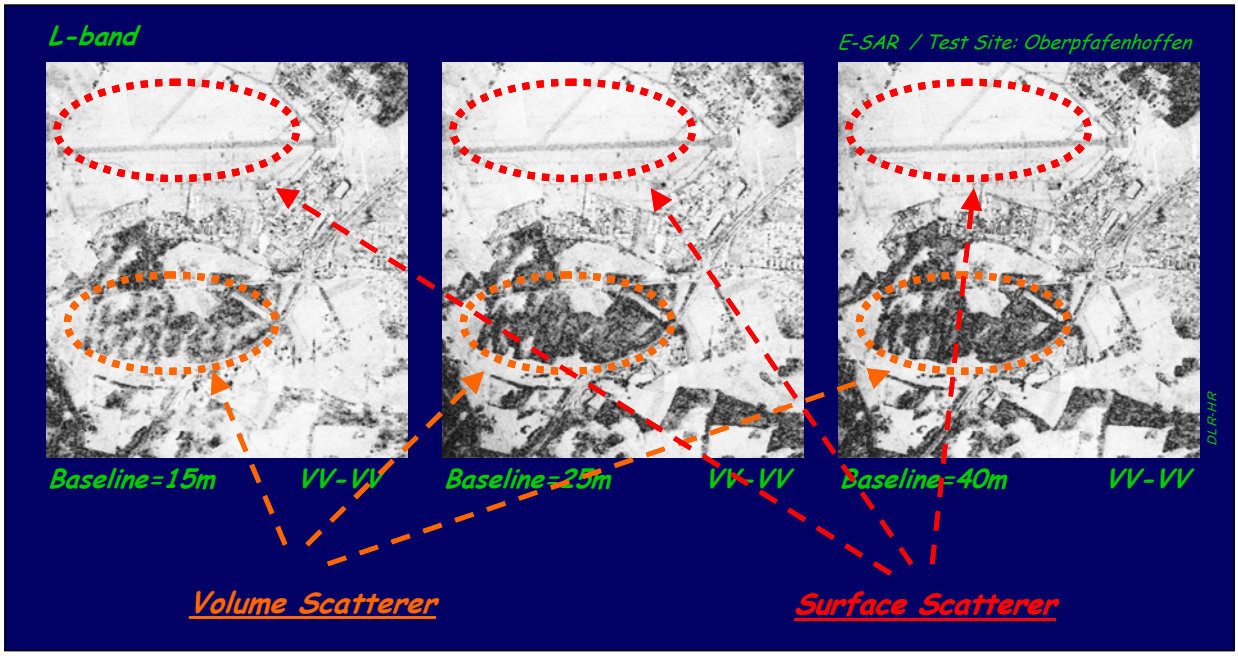

Figure 9 Interferometric coherence images at three different baselines.

2.3 RANDOM VOLUME (RV)

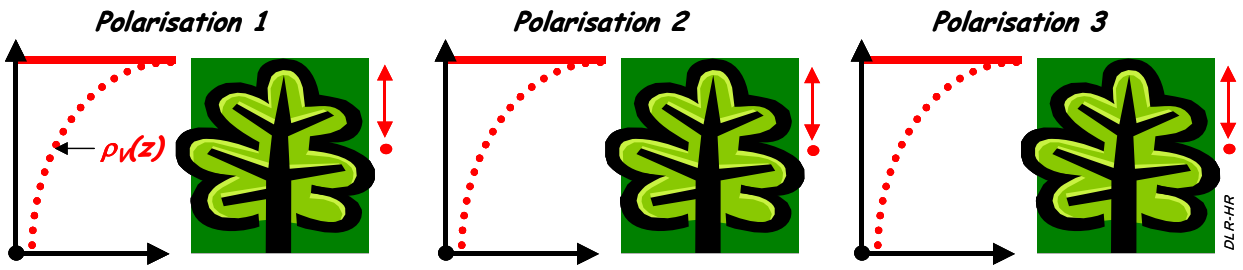

Figure 10 Vertical distribution of scatterers at three different polarisations according to the RV model.

In the case of a *Random Volume (RV)* the volume particles are characterised by a random orientation distribution that makes wave propagation through the volume polarimetric isotropic, i.e., independent of the polarisation state of the wave. All polarisations propagate through the volume with the same refraction and extinction coefficient $\sigma \neq \sigma(\vec{w})$. In consequence, the effective vertical distribution of scatterers $\rho_V(z)$ do not change with polarisation (as indicated in Figure 10), so that the interferometric volume coherence is the same for all polarisations:

$$\tilde{\gamma}_{Vol} = \exp(i\varphi_0)\frac{\int_0^{h_V} \exp(z\sigma/\cos(\theta))\exp(-2i\kappa_z z')dz'}{\int_0^{h_V} \exp(z\sigma/\cos(\theta))dz'} \neq \tilde{\gamma}_{Vol}(\vec{w}) \tag{40}$$

The effective phase center and penetration depth are the same for all polarisations and depend on the extinction coefficient σ. For the limit of zero extinction coefficient, $\gamma_{Vol}(\vec{w})$ becomes the well known sin(x)/x decorrelation function

$$\tilde{\gamma}_{Vol} = \exp(i\varphi_0 + i\kappa_z h_V/2)\frac{\sin(\kappa_z h_V/2)}{\kappa_z h_V/2} \tag{41}$$

while for $\sigma = \infty$, the case of an impenetrable volume, only surface scattering on the top of the volume occur, without any volume decorrelation

$$\tilde{\gamma}_{Vol} = \exp(i\varphi_0 + i\kappa_z h_V) \tag{42}$$

As the volume decorrelation term is independent on polarisation, only SNR and temporal decorrelation effects may make the overall coherence to be different at different polarisations

$$\tilde{\gamma}(\vec{w}) = \gamma_{SNR}(\vec{w})\ \gamma_{Temp}(\vec{w})\ \exp(i\varphi_0)\frac{\int_0^{h_V} \exp(z\sigma/\cos(\theta))\exp(-2i\kappa_z z')dz'}{\int_0^{h_V} \exp(z\sigma/\cos(\theta))dz'} \tag{43}$$

However, potential SNR decorrelation effects can be identified, as they do not effect the location of the individual phase centers and increase only the variance of the interferometric phase.

Optimal Polarisations:

The polarimetric coherence optimisation problem - in the absence of temporal decorrelation effects - reduces to a pure SNR optimisation problem as $\gamma_{SNR}(\vec{w})$ is the only polarisation dependent parameter (ignoring the temporal decorrelationcontribution $\gamma_{Temp}(\vec{w})$).

2.4 ORIENTED VOLUME (OV)

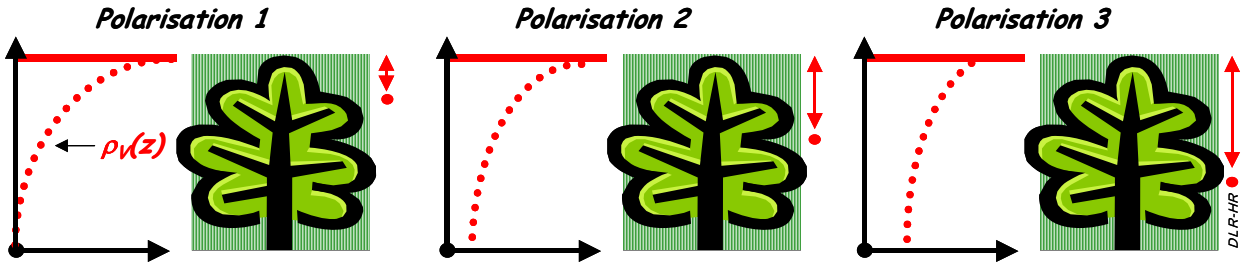

Figure 11 Vertical distribution of scatterers at three different polarisations according to the OV model.

Volumes with particles characterised by an orientation correlation are called *Oriented Volumes (OV)*. Due to the orientation of the volume particles, propagation becomes anisotropic, and waves at different polarisations propagate with different complex (propagation) wave-numbers through the volume.
Wave propagation through an OV is completely described by the eigenpolarisations of the volume, i.e. the polarisations along which the incident wave does not change its polarisation state as it propagates through the volume. Each eigenpolarisation is characterised by its own complex (propagation) wave-numbers describing refraction and attenuation (i.e. extinction). The propagation of any other polarisation state can be described by decomposing the polarisation state into two components aligned with the eigenpolarisations, and propagate them along the eigenpolarisations. Accordingly, due to the different refraction of the two components the polarisation state of the wave changes with wave propagation through the volume – in this sense the OV acts as a polarisation filter.
The eigen-polarisations are given by the eigenvectors of the average forward scattering matrix. For most natural media faced in radar remote sensing, the eigenpolarisations can be assumed to be orthogonal and linear polarisation states (i.e. the media have a symmetric forward scattering matrix).
In the case of OV, the effective vertical distribution of scatterers $\rho_V(z)$ changes with polarisation due to the change of the wave extinction coefficient (see Figure 11), and consequently the interferometric volume coherence becomes a function of polarization

$$\tilde{\gamma}_{Vol}(\vec{w}) = \exp(i\varphi_0)\frac{\int_0^{h_V}\exp(z\sigma(\vec{w})/\cos(\theta))\exp(-2i\kappa_z z')dz'}{\int_0^{h_V}\exp(z\sigma(\vec{w})/\cos(\theta))dz'} \qquad (44)$$

Accordingly, with increasing extinction the effective phase center moves towards the top of the volume, the effective volume seen by the interferometer decreases, and the interferometric coherence increases.

One direct consequence arising from this extinction-coherence relation is the fact that for any orthogonal polarisation basis the interferometric coherence of the cross-polar channels will be ranked between the coherences of the co-polar channels as

$$\tilde{\gamma}_{Vol}(\vec{w}_{mm}) \geq \tilde{\gamma}_{Vol}(\vec{w}_{mn}) \geq \tilde{\gamma}_{Vol}(\vec{w}_{nn}) \text{ with } \quad \sigma_m \geq \sigma_n \tag{45}$$

While the co-polar channels refer to waves that propagate through the volume two times (in incident and back-scattering direction) with the same extinction coefficient (i.e. $\vec{w}_{nn}$ propagates with σ_m in incident and back-scattering direction while $\vec{w}_{nn}$ with σ_n), the cross-polar channel refer to a propagation in incidence direction with σ_m (or σ_n) and in backscattering direction with σ_n (or σ_m). Thus the effective extinction for the cross-polar channel σ_{mn} is given by the mean value of two extinction values for the orthogonal co-polar channels

$$\sigma_{mn} = \frac{\sigma_m + \sigma_n}{2} \qquad \text{where} \qquad \sigma_m \geq \sigma_{mn} \geq \sigma_n \tag{46}$$

leading to the ranking of (45).

Optimal Polarisations

Based on the considerations above, one may expect that in the case of an OV, the maximum / minimum interferometric coherence will be obtained for the polarisation state associated to the maximum / minimum extinction coefficient. Indeed, it can be proved analytically that the optimal polarisations obtained from the coherence optimisation are the eigenpolarisations of the OV ($\vec{w}_A$ and $\vec{w}_B$) that correspond to the maximum / minimum extinction values

$$\tilde{\gamma}_{Vol}(\vec{w}_{Opt1} = \vec{w}_A) = \frac{2\sigma_A \exp(i\varphi_0)}{\cos\theta_0[\exp(2\sigma_A/\cos\theta_0) - 1]} \int_0^{h_V} \exp(i\kappa_z z') \exp\left(\frac{2\ \sigma_A z'}{\cos\theta_0}\right) dz' \tag{47}$$

$$\tilde{\gamma}_{Vol}(\vec{w}_{Opt2} = \vec{w}_M) = \frac{2\sigma_M \exp(i\varphi_0)}{\cos\theta_0[\exp(2\sigma_M/\cos\theta_0) - 1]} \int_0^{h_V} \exp(i\kappa_z z') \exp\left(\frac{2\ \sigma_M z'}{\cos\theta_0}\right) dz' \tag{48}$$

$$\tilde{\gamma}_{Vol}(\vec{w}_{Opt3} = \vec{w}_B) = \frac{2\sigma_B \exp(i\varphi_0)}{\cos\theta_0[\exp(2\sigma_B/\cos\theta_0) - 1]} \int_0^{h_V} \exp(i\kappa_z z') \exp\left(\frac{2\ \sigma_B z'}{\cos\theta_0}\right) dz' \tag{49}$$

σ_A and σ_B are the eigen-extinctions (i.e. the extinction coefficients along the eigenpolarisations) that are the maximum / minimum volume extinction values and

$$\sigma_M = \frac{\sigma_A + \sigma_B}{2} \tag{50}$$

Note that - assuming orthogonal eigen-polarisations – the optimal polarisations obtained from the coherence optimisation algorithm are orthogonal to each other.

3 COMBINED SURFACE AND VOLUME SCATTERING

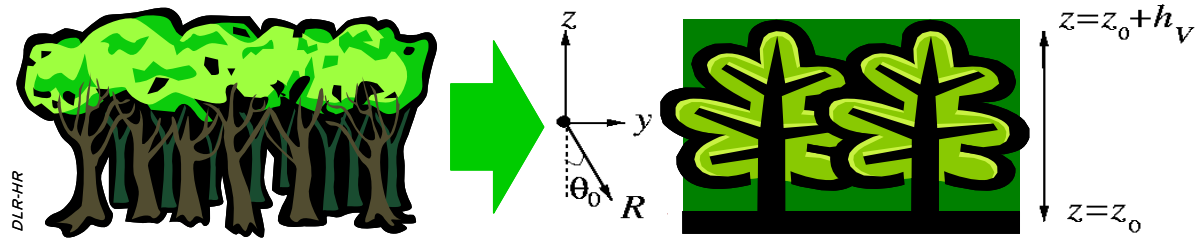

Figure 12 Random Volume over Ground Scattering Model.

In the case of vegetation scattering at lower frequencies, a realistic scattering scenario has to consider both, vegetation layer and ground interactions. The simplest way to model such a scenario is by combining a volume with a ground scatterer. Accordingly, the vegetation is modeled as a single layer of thickness h_V containing a volume with scattering particles characterised by a scattering amplitude per unit volume m_V. This volume, as shown schematically in Figure 12, is located over a ground scatterer positioned at $z=z_0$ with scattering amplitude m_G. The ground is seen through the vegetation layer by an interferometric system operating at wavelength λ with physical baseline B under a mean incident angle θ.
In this case, the complex interferometric coherence $\tilde{\gamma}(\vec{w})$ after range spectral filtering, may be written as

$$\tilde{\gamma}(\vec{w}) = \gamma_{SNR}\gamma_{Temp}\exp(i\varphi_0)\frac{\tilde{\gamma}_V + m(\vec{w})}{1 + m(\vec{w})} \tag{51}$$

where $\tilde{\gamma}_V$ denotes the complex coherence for the volume alone, which depends on the extinction coefficient for the random volume, and it's thickness h_V as

$$\tilde{\gamma}_V = \frac{I}{I_0} \quad \text{where} \quad I = \int_0^{h_V} \exp(i\kappa_z z')\exp\left(\frac{2\,\sigma\,z'}{\cos\theta_0}\right)dz' \qquad I_0 = \int_0^{h_V} \exp\left(\frac{2\,\sigma\,z'}{\cos\theta_0}\right)dz' \tag{52}$$

φ_0 is the phase related to the ground topography and m the effective ground-to-volume amplitude ratio accounting for the attenuation through the volume

$$m(\vec{w}) = \frac{m_G(\vec{w})}{m_V(\vec{w})I_0} \tag{53}$$

The extinction coefficient corresponds to a mean extinction value for the vegetation layer. According to (51), the effective phase center is located above the ground at a height that depends on the ground-to-volume amplitude ratio m as well as the attenuation length of the vegetation layer.
Equations (51) and (53) address the volume over ground scattering problem as a four parameter problem regarding: 1) the volume thickness h_V, 2) the volume extinction coefficient σ, 3) the

effective ground-to-volume amplitude ratio m, and, 4) φ_0 the phase related to the underlying topography.
In the absence of a ground scattering contribution, $m = 0$, (51) leads to the volume only case discussed in the previous section

$$\tilde{\gamma} = \gamma_{SNR}\gamma_{Temp}\exp(i\varphi_0)\ \tilde{\gamma}_V \tag{54}$$

In the other limit case of a very strong ground scattering contribution, $m(\vec{w}) \mapsto \infty$ and (52) leads to the surface scattering case

$$\tilde{\gamma}(\vec{w}) = \gamma_{SNR}\gamma_{Temp}\exp(i\varphi_0) \tag{55}$$

Based now on the volume's propagation properties with respect to the polarisation state of the incident wave two cases:

- ***Random Volume over Ground (RVoG):*** The propagation (i.e. extinction) through the volume is independent of polarisation
- ***Oriented Volume over Ground (OVoG):*** The propagation (i.e. extinction) through the volume changes with polarisation

These two cases will be discussed in the next sections.

3.1 RANDOM VOLUME OVER GROUND (RVOG)

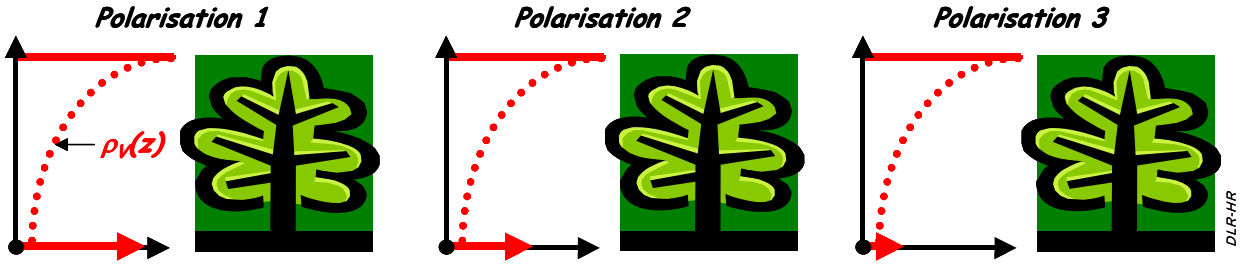

Figure 13 Vertical distribution of scatterers at three different polarisations according to the RVoG model.

In the case of the *Random Volume over Ground (RVoG)* model the propagation through the volume is independent of polarisation: i.e., $\sigma \neq \sigma(\vec{w})$. In consequence, the volume only complex coherence $\tilde{\gamma}_V$ becomes independent of polarisation

$$\tilde{\gamma}_V = \frac{I}{I_0} \neq \tilde{\gamma}_V(\vec{w}) \quad \text{where} \quad \begin{aligned} I &= \int_0^{h_V} \exp(i\kappa_z z')\exp\left(\frac{2\ \sigma\ z'}{\cos\theta_0}\right)dz' \\ I_0 &= \int_0^{h_V} \exp\left(\frac{2\ \sigma\ z'}{\cos\theta_0}\right)dz' \end{aligned} \tag{56}$$

The only parameter of the model that depends now on the polarisation state $\vec{w}$ is the ground-to-volume amplitude ratio $m(\vec{w})$. And it is the variation of $m(\vec{w})$ with polarisation the reason that makes the overall interferometric coherence $\tilde{\gamma}_V(\vec{w})$ to be a function of polarization

$$\tilde{\gamma}(\vec{w}) = \gamma_{SNR}\gamma_{Temp}\exp(i\varphi_0)\frac{\tilde{\gamma}_V + m(\vec{w})}{1 + m(\vec{w})} \tag{57}$$

Accordingly, the location of the effective phase center depends on the value of $\tilde{\gamma}_V$ (that again depends on the height and the extinction of the vegetation layer) and the ground-to-volume amplitude ratio $m(\vec{w})$.
Regarding now the vertical distribution of the scatterers at different polarisations, the distribution of the volume scatterers - defined by the volume height and extinction – does not change with polarisation, and the overall vertical distribution changes due to the variation of the ground scattering component. This makes the volume decorrelation to be polarisation dependent.
Finally note that, the difference between the phase centers of interferograms formed at different polarisation is directly related to the difference of the corresponding ground-to-volume amplitude ratios.

The RVoG model has been used successfully in several vegetation parameter inversion scenarios from multiparameter InSAR data.

Optimal Polarisations
As the ground-to-volume amplitude ratio $m(\vec{w})$ is the only parameter that changes with polarisation according to the RVoG model, coherence optimisation is based on the variation of $m(\vec{w})$. Indeed, it can be shown that the optimum coherences corresponds to the polarisations that maximise / minimise $m(\vec{w})$:

$$\tilde{\gamma}_{Vol}(\vec{w}_{Opt1} = \vec{w}_A) = \frac{2\sigma_A \exp(i\varphi_0)}{\cos\theta_0[\exp(2\sigma_A/\cos\theta_0) - 1]}\int_0^{h_V}\exp(i\kappa_z z')\exp\left(\frac{2\ \sigma_A z'}{\cos\theta_0}\right)dz' \tag{58}$$

$$\tilde{\gamma}_{Vol}(\vec{w}_{Opt2} = \vec{w}_M) = \frac{2\sigma_M \exp(i\varphi_0)}{\cos\theta_0[\exp(2\sigma_M/\cos\theta_0) - 1]}\int_0^{h_V}\exp(i\kappa_z z')\exp\left(\frac{2\ \sigma_M z'}{\cos\theta_0}\right)dz' \tag{59}$$

$$\tilde{\gamma}_{Vol}(\vec{w}_{Opt3} = \vec{w}_B) = \frac{2\sigma_B \exp(i\varphi_0)}{\cos\theta_0[\exp(2\sigma_B/\cos\theta_0) - 1]}\int_0^{h_V}\exp(i\kappa_z z')\exp\left(\frac{2\ \sigma_B z'}{\cos\theta_0}\right)dz' \tag{60}$$

Note that in general the optimal polarisations obtained from the coherence optimisation algorithm are not orthogonal to each other.

3.2 ORIENTED VOLUME OVER GROUND (OVOG)

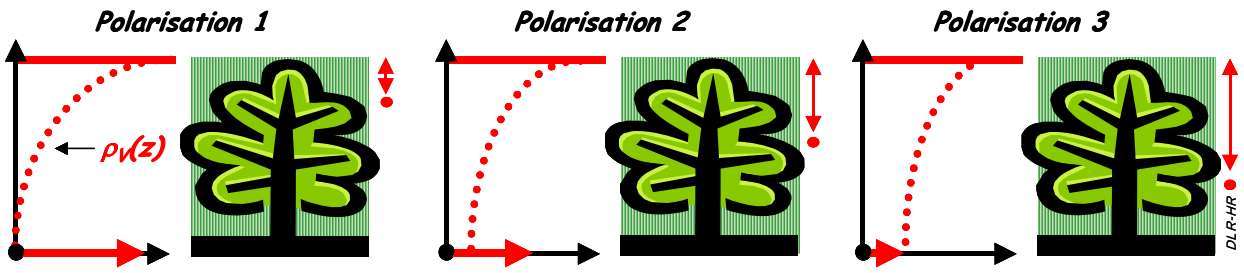

Figure 14 Vertical distribution of scatterers at three different polarisations according to the OVoG model.

In the case of the Oriented Volume over Ground (*OVoG*) model, the propagation through the volume becomes a function of polarisation, i.e. $\sigma = \sigma(\vec{w})$. Accordingly, the volume only complex coherence $\tilde{\gamma}_V$ becomes a function of polarization

$$\tilde{\gamma}_V(\vec{w}) = \frac{I(\vec{w})}{I_0(\vec{w})} \qquad \text{where} \qquad I(\vec{w}) = \int_0^{h_V} \exp(i\kappa_z z') \exp\left(\frac{2\ \sigma(\vec{w})\ z'}{\cos\theta_0}\right) dz' \qquad I_0(\vec{w}) = \int_0^{h_V} \exp\left(\frac{2\ \sigma(\vec{w})\ z'}{\cos\theta_0}\right) dz' \tag{61}$$

The fact that the polarisation state of an incident wave changes by its propagation through the volume (except it coincides with the one of the volume eigenpolarisations) makes the ground seen through the volume by the nterferometer as to be seen through a polarisation filter. In the combined ground and volume coherence term now, both the volume and the surface (ground-to-volume amplitude $m(\vec{w})$) become polarisation dependent, and the overall interferometric coherence $\tilde{\gamma}(\vec{w})$ becomes

$$\tilde{\gamma}(\vec{w}) = \gamma_{SNR}\gamma_{Temp} \exp(i\varphi_0) \frac{\tilde{\gamma}_V(\vec{w}) + m(\vec{w})}{1 + m(\vec{w})} \tag{62}$$

Different than in the case of the OvoG, here a change in polarisation changes the distribution of scatterers within the volume as well as the ground scattering component as indicated in Figure 14. The difference between the phase centers of interferograms at different polarisations depends now on the difference between the corresponding extinction coefficients as well as on the difference of the corresponding ground-to-volume amplitude ratios.

Optimal Polarisations

In the case of an OVoG the coherence optimisation procedure has two polarisation dependent parameters to vary: the extinction coefficient $\sigma(\vec{w})$ and the ground-to-volume amplitude ratio $m(\vec{w})$. For polarisations with higher extinction values the volume scattering occurs more on the upper volume part while at the same time ground scattering becomes stronger attenuated moving the common scattering center towards the top. In this case, a strong ground contribution can increase volume decorrelation while a soft ground contribution will decrease volume decorrelation. In the case of polarisations with low extinction values the volume scattering occurs deeper within the volume while at the same time ground scattering becomes more “visible”. Here, a strong ground

contribution decreases volume decorrelation while a soft ground contribution increases volume decorrelation.
Finally, due to the presence of the ground, the optimal polarisations have no longer to be orthogonal.